Effect of gamma-irradiation on (PEO/PVP)/Au nanocomposite: Materials for electrochemical and optical applications

A.M. Abdelghany [a], E.M. Abdelrazek [b,c], S.I. Badr [c], M.A. Morsi [d,*]

[a] *Spectroscopy Department, Physics Division, National Research Center, 33 ElBehouth St., Cairo 12311, Egypt*
[b] *Department of Physics, Faculty of Science at Al-Ula, Taibah University, Saudi Arabia*
[c] *Physics Department, Faculty of Science, Mansoura University, Mansoura 35516, Egypt*
[d] *Engineering Basic Science Department, Faculty of Engineering, Egyptian Russian University, Cairo 11829, Egypt*

ABSTRACT

Gold nanoparticles (Au NPs) have been successfully biosynthesized by *Chenopodium murale* (*C. murale*) leaf extract. Au NPs were incorporated within polyethylene oxide (PEO)/polyvinyl pyrrolidone (PVP) blend by casting method. Prepared samples were characterized before and after subjecting to successive gamma-irradiation doses (1, 2, 3, 4, 5 Mrad). XRD confirmed the semicrystalline nature of blend which was largely decreased after embedding Au NPs and subsequently through high irradiation doses. Before irradiation, FT-IR spectra revealed presence of main vibrational bands due to both PEO and PVP. After irradiation, FT-IR spectra indicated the existence of structural rearrangements in the polymeric matrix due to irradiation process. UV/vis spectra indicated presence of n–π* transition results from single-bond in the backbone of blend and showed a visible band at 531 nm attributed to the surface plasmon resonance of Au NPs that is largely affected by irradiation dose. The values of optical parameters were enhanced due to embedding Au NPs and varied according to the irradiation dose. TEM images showed that particle size range was reduced from 1 to 34 nm for nanocomposite to 4–22 nm after exposure to γ-radiations of 5 Mrad. TGA analysis showed an improvement for the thermal stability of nanocomposite sample after gamma-rays treatment.

© 2016 Elsevier Ltd. All rights reserved.

1. Introduction

Nanocomposite materials have been of great interest for a number of reasons, which include the materials development with innovative thermal and mechanical properties, optimization of processes and new applications, and the understanding of fundamental phenomena occurring at the nano-scale level [1]. These materials exhibit unique electrical mechanical and optical properties making them valuable for applications in areas like photo-imaging, optics and sensor design, information storage, patterning, and as antimicrobial coatings [2,3].

Polymer blending is a simple and practical method to form new materials. The samples produced by blending of two or more polymers usually result in modified physical and mechanical properties compared to samples made of the initial components. In addition, the blending of synthetic polymers may enhance the cost-performance ratio of the resulting films [4].

Polyethylene oxide (PEO) has a high thermal stability and is a semi-crystalline polymer which has both crystalline and amorphous phases at room temperature due to its high regularity of its structural unit. PEO is a linear polymer with enteric linkages (i.e. ether group C—O—C) and can solvate different types of inorganic salts. But, a high ordering of

PEO structure restricts its conductivity so it must be coupled with amorphous polymer. Polyvinyl pyrrolidone (PVP) has been taken as a partner for PEO in preparing polymer blend, due to its individual characteristics. PVP is an amorphous polymer, which can allow faster ionic mobility compared with other semi-crystalline polymers having low scattering losses for different applications. Because of the existence of carbonyl group (C=O) in the PVP side chains, it produces a variety of complexes with different inorganic salts. Another utility of choosing PVP is that it can be thermally cross-linked, producing a good thermal stability and mechanical strength of the blended material and also due to the PVP solubility in water which is a common solvent of PEO, so it is favorable to eliminate phase separation in the polymers of blend [5–7]. Also, PVP is a suitable capping agent for nanoparticles (NPs) due to the presence of both carbonyl group (˘C=O) and >N— that make anchoring for NPs and having long chain. The functional groups having lone pairs of electrons help in metal NPs stabilization at their surface by covalent interaction, while the polymer chain binds metal NPs aggregation through steric hindrance [8].

Gold nanoparticles (Au NPs) have been widely studied in the past 10 years due to their unique properties, such as quantum size effect, catalytic, and optical properties [9–11] which make them suitable materials for potential applications in various fields. Au NPs have been found to play an important role in many gas sensing processes, catalytic and nano-medicine applications [11]. Also, Au NPs have high performance

* Corresponding author.
  E-mail address: m.a_morsi@yahoo.com (M.A. Morsi).

catalysts for the oxygen reduction reaction (ORR) in electrochemical applications, such as fuel cell, which gives decrease to the larger over-potential and higher current density [12].

Many physical properties of polymeric materials such as optical, structural, electrical, thermal, and mechanical properties are modified, after subjecting to γ-irradiation. These modifications are because of the chemical bond scissions and/or cross-linking induced by high-energetic radiation [13]. When an ionization radiation passes through a polymeric material, excitation and ionization for the molecules of material are existed. These lead to breaking of original bonds, chain scission, radical formation and cross-linking in polymeric material. Scission and cross-linking not only depend upon polymer structure but also upon the energy deposited per unit track length (LET). This, in turn, tends to modify the structure and optical properties of polymers [14].

The aim of present study is to analyze structural, morphological and physical properties of (PEO/PVP) blend/Au nanocomposite at different irradiation doses after embedding biosynthesized Au NPs by *Chenopodium murale* extract (*C. murale*) instead of using common hazardous chemicals. The obtained samples are suitable in electrochemical application, as a solid polymer electrolyte, and optical applications.

2. Experimental

2.1. Materials

The leaf of *C. murale* was collected from Mansoura city, Dakahlia governorate, Egypt during December 2014. Tetrachloroauric (III) acid trihydrate (HAuCl$_4$·3H$_2$O, 99.5% GR for analysis) was obtained from Merck, Germany. All the chemicals and solvent used in this study were of analytical grade. Both PEO supplied from ACROS, New Jersey, USA with molecular weight (M.W.) ≈ 40,000 g/mol and PVP from SICO Research Laboratories Pvt. Ltd, Mumbai, India with M.W. ≈ 72,000 g/mol were used as a basic polymeric materials. The used solvent was double distilled water.

2.2. Preparation of C. murale extract and biosynthesis of Au NPs

The leaves of *C. murale* were washed fully thrice with double distilled water. In a 500 ml Erlenmeyer flask, 20 g of washed leaves boiled in 50 ml double distilled water for 30 min at 100 °C. Then the leaf extract was collected in a separate conical flask by a standard filtration method i.e. Whatman No. 40 filter paper. 100 ml of 5×10^{-3} M aqueous solution of gold chloride was prepared in a Stoppard Erlenmeyer flask and 2 ml of leaf extract (0.2 g/ml) was added at room temperature and pH value of the solution was adjusted to 10 with an aqueous solution of 0.1 M NaOH. After one hour in dark, the solution changes from yellow to a pinkish-red solution as shown in Fig. 1, which indicated the formation of Au NPs [2,15,16]. The

resulting solution was centrifuged at 13,000 rpm for 5 min and stored at 4 °C for further use. Finally, powdered pinkish-red colored solid appeared at the bottom of centrifuged tube. This was followed by separation and washing of the powder with double distilled water five times. The powder was then air dried and kept for further use.

2.3. Preparation of PEO/PVP/Au nanocomposite films

Polymer blend electrolyte films were prepared by solution cast technique. A quantity of PEO and PVP (70/30 wt%) was dissolved in double distilled water separately and then the polymer blend solution was stirred continuously at room temperature until a homogenous viscous liquid was formed. Further, 3.6 mg of prepared Au NPs were added to the PEO/PVP polymer solution under continuous stirring for 24 h. Finally, viscous solutions were poured into polypropylene dishes and the common solvent was allowed to evaporate slowly at room temperature for 2 days to obtain free-standing polymer electrolyte films at the bottom of dishes. The obtained films were stored in highly evacuated desiccators to avoid any moisture absorption. Film thickness in the range of 0.07–0.09 mm was obtained.

2.4. γ-Irradiation process

Gamma 1 (type J-3600, Canada, Ltd.) for atomic energy, located at the National Center for Radiation Research and Technology (Cairo, Egypt), was used. A ^{60}Co source, with an activity of 137,000 Ci, was used for the γ-irradiation of the PEO/PVP/Au nanocomposite films. The irradiation doses (1, 2, 3, 4 and 5 Mrad) were measured with radiochromic dye film on Perspex. The dose rate was 2.76 kGy/h. The overall error in the dose measurements did not exceed ±4%.

2.5. Measurements

X-ray diffraction scans were obtained using DIANO corporation-USA equipped using Cu Kα radiation (λ = 1.5406 Å, the tube operated at 30 kV, the Bragg's angle (2θ) in the range of 5–80°. FT-IR absorption spectra were carried out for different films using the single beam Fourier transform-infrared spectrometer (Nicolet *iS*10, USA) at room temperature in the spectral range of 4000–400 cm^{-1}. Ultraviolet/visible (UV/vis) absorption spectra were measured in the wavelength region of 200–1000 nm using spectrophotometer (V-570 UV/VIS/NIR, JASCO, Japan). Transmission electron microscope (TEM), (JEOL-JEM-1011, Japan) was used to study the size, shape and distribution of the biosynthesized Au NPs. TGA curves for the studied samples were recorded using (NETZSCH, STA 409CD, Germany) in temperature range from room temperature to 700 °C and the heating rate was 10 °C/min in the existence of nitrogen as inert atmosphere.
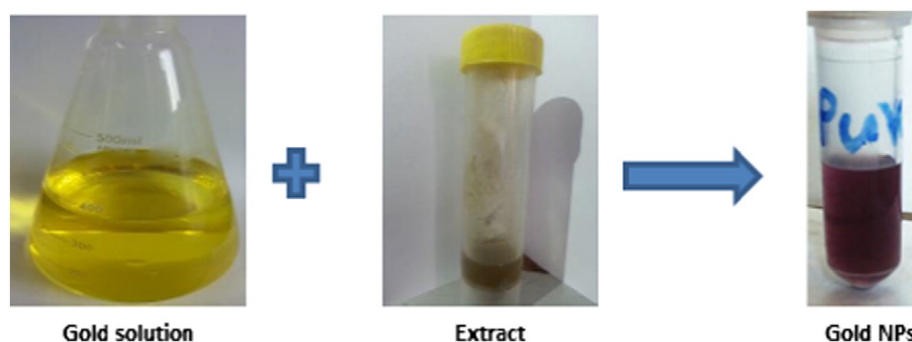

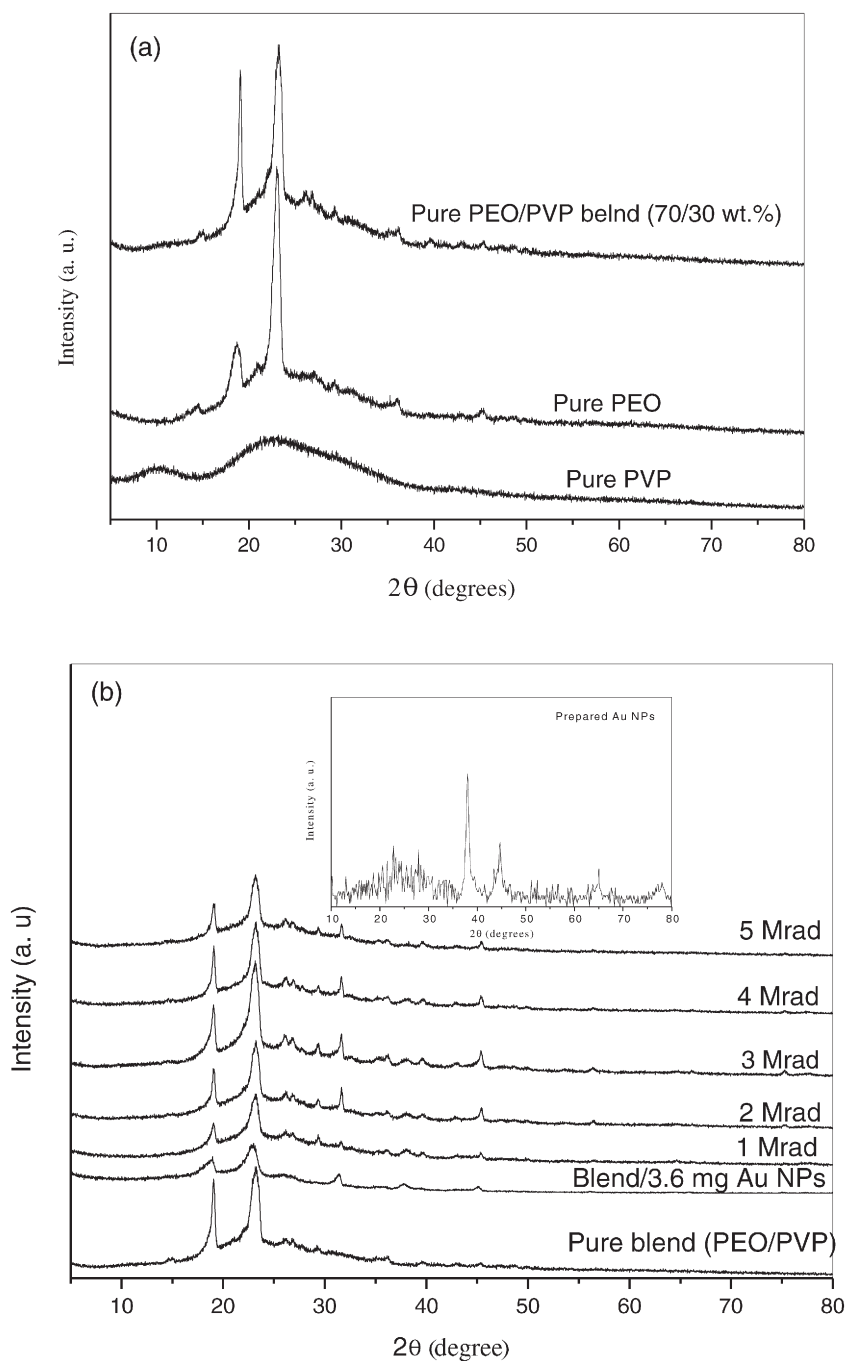**Fig. 1.** Biosynthesis of Au NPs by *C. murale* leaf extract.

Fig. 2. a–b. XRD scans of pure PVP, pure PEO, PEO/PVP blend, PEO/PVP/Au nanocomposite before and after γ-irradiation at different doses and Au NPs crystalline phases.

3. Results and discussion

3.1. X-ray diffraction analysis XRD

Fig. 2.a shows the XRD spectra for pure PEO, PVP and pure blend. The spectrum of PEO confirms the semi-crystalline nature of PEO and exhibits peaks at 23.11°, 18.57° and 26.91° which are referred to (112), (120) and (222) planes [PCPDF File nos. 49-2200 and 49-2201] [5,6,17] respectively. Also, there are many low intense peaks at 14.40°, 20.74°, 27.01°, 29.24°, 36.11° and 45.40°. While, the spectrum of PVP confirms the amorphous nature of PVP and have two broad peaks at 13° and 21° [6,18]. The spectrum of pure blend has two main crystalline peaks at 19° and 23° accompanied with low intense peaks at 25.26°, 26.92°, 29.30°, 36.25° and 45.36°. These previous peaks arisen from the crystalline phases of PEO. This observation confirms the semi-crystalline nature of PEO/PVP blend.

Fig. 2.b shows the XRD of pure PEO/PVP (70/30 wt%) blend, PEO/PVP/Au nano-composites (3.6 mg Au NPs) and its irradiation at different doses (1, 2, 3, 4 and 5 MR). When Au NPs are added to PEO/PVP blend, the intensity of crystalline peaks is largely decreased and their width increased. This result indicates that there is a coordination interaction between Au NPs and ether group (C—O—C) of PEO and/or carbonyl group (C=O) of PVP of polymer blend. Thus, the intermolecular interaction between the chains of polymer blend is deceased which results in a marked decrease in the degree of crystallization and increase in the amorphous region within polymer blend matrix.

XRD spectrum for the crystalline phases of Au NPs is shown in Fig. 2.b. The patterns of Bragg reflection appearing at 2θ = 38° (111),

42° (200), 64° (220) and 78° (311) are indexed for the face-centered cubic FCC structure of Au NPs (JCPDS File No. 4-0784) [2,16,19]. From Fig. 2.b, there is a new crystalline peak at $2\theta \approx 38°$ where its position coincides with the position of crystalline phase at $2\theta = 38°$ in the XRD pattern of Au NPs. This confirms the existence of Au NPs crystallites within the polymeric matrix. Also, a new sharp peak appears at $2\theta \approx 31.5°$. This appearance is resulting from the crystalline phase within the polymeric matrix, due to the existence of Au NPs. This scattering angle may be associated with the (200) and (112) reflections, respectively [20]. This observation shows that there are structural changes within PEO/PVP matrix and forms blend-Au complex.

As the irradiation doses increase from 1 to 3 Mrad, the intensity of two main crystalline peaks at $2\theta = 19°$ and $23°$ increases gradually. This observation may show the fact that the polymeric matrix suffers from some kind of structural rearrangement because irradiation treatments that lead to an increase the degree of crystallinity [21]. The increase of the degree of crystallinity for the irradiated samples occurs because of the irradiation absorption and transference of energy to the polymer, leading to bond cleavage, ionization, and/or recombination reactions. Accordingly, the previously dislocated atom, in the outer most zones of the crystallites, will return to their normal crystalline sites, enhancing the degree of crystallinity [22]. It is well known that, the molecular chains of PEO/PVP are held together by the H-bonding [23]. Due to irradiation by γ-rays, these bonds break and the molecular chains are partly free to rotate. The rotation probably happens in the direction making the directions (120) and (112) richer in the atoms number. Thus the increase in the intensity of the diffraction peaks at $2\theta = 19°$ and $23°$ can be understood. Also, it is obvious that the intensity of peaks at $2\theta = 31.5°$, $38°$ and $45°$ increases up to γ-irradiation dose of 3 Mrad, which denotes the increase in the crystalline phase in nanocomposites because of increase in the size Au NPs and particles growth.

If the irradiation dose increases from 3 to 5 Mrad the intensity of two main diffraction peaks decreases and broadens gradually in accordance with their small grain sizes. These nanocrystals have lesser lattice planes compared to bulk, which contributes to the broadening of the peaks in the diffraction pattern. This means that the irradiation process at high doses causes a decrease in the degree of crystallinity due to free radical formation. The formation of radicals includes bond cleavage, such as chain scission and/or hydrogen elimination, which may result in a decrease in polymer molecular weight, cross-linking by recombination reaction, or other side reactions, such as formation of double bond. It is believed that free radicals (gathered near the crystallite boundaries) dislocate the neighboring atoms out of their crystal sites. This sets up a shell of deformed pattern in the outermost zone of the crystallite, which decreases the effective crystalline volume. So, the relatively lower degree of crystallinity of irradiated samples at high doses is explained [22]. The decrease in intensity and the slight increase in the broadness of diffraction peaks show the decrease in the size of Au NPs which is also confirmed by UV/vis spectroscopy and TEM micrographs.

The crystalline fraction of the samples (X_c), is determined by Hermans–Weidinger method [24]:

$$X_c = \frac{A_{crystalline}}{A_{crystalline} + A_{amorphous}} \quad (1)$$

where $A_{crystalline}$ and $A_{amorphous}$ are the areas of crystalline reflections and amorphous halo, respectively and K is constant and can be set to unity for comparative purposes. Due to small amount crystalline material in samples, these measurements may not accurately reflect absolute degree of crystallinity, but reproducible relative values are consistently obtained. Table 1 shows change of crystalline fraction of samples as a function of Au concentration and irradiation doses. From Table 1, it is obvious that addition of Au NPs to PEO/PVP blend increases amorphous fraction and decreases degree of crystallinity for PEO/PVP blend. The degree of crystallinity is highest at irradiation dose 3 Mrad compared to other irradiated samples. Also, the average crystalline size of Au NPs is estimated for blend/3.6 mg Au NPs, blend/3.6 mg Au NPs/3 Mrad and blend/3.6 mg Au NPs/5 Mrad, at 2θ values $38°$ using Debye-Scherrer formula [21] are 21.87, 24.63 and 10.68 nm, respectively which is confirmed by TEM micrographs.

3.2. Fourier transform infrared analysis FT-IR

Fig. 3.a shows the FT-IR spectra of pure PEO, PVP and pure (PEO/PVP) blend while Fig. 3.b depicts FT-IR spectra for pure blend, (PEO/PVP) blend/3.6 mg Au NPs nanocomposite and its γ-irradiation at different doses in the spectral range 4000–400 cm^{-1}.

FT-IR spectra for both PEO and PVP polymers are in coincidence with those reported previously [5,6,25,26]. From Fig. 6, PEO spectrum has sharp band at 2885 cm^{-1} which is assigned to C—H asymmetric stretching of methylene group. CH_2 scissoring and CH_2 asymmetric bending are clearly observed at 1461 cm^{-1} and 1345 cm^{-1}, respectively. The relatively small band at 1240 cm^{-1} is due to CH_2 symmetric twisting. The absorption band located at 1110 cm^{-1} corresponds to C—O—C stretching mode. The bands at 956 and 840 cm^{-1} are due to CH_2 asymmetric rocking motion with some contribution from C—O stretching.

The spectrum of pure PVP displays a broad band at about 3425 cm^{-1} and is corresponded to the stretching vibration of hydroxyl group (OH) of PVP and can be considered a source of Hydrogen bond in blending with PEO. The absorption band located at 2955 cm^{-1} corresponds to CH_2 asymmetric stretching vibration. The vibrational band at about 1660 cm^{-1} corresponds to C=O stretching of PVP. Very small absorption band at about 1500 cm^{-1} refers to the characteristic vibration of C=N (pyridine ring). C—H bending of CH_2 or OH bending is located at 1460 cm^{-1} while, the band at 1435 cm^{-1} is assigned to CH_2 scissoring vibrations. The vibrational band observed at 1290 cm^{-1} may be attributed to CH_2 twisting or wagging of PVP.

From Fig. 3.a, the coexistence of both (C—O—C) group of PEO and (C=O) group of PVP in the FT-IR spectrum of pure blend shows that PEO and PVP are miscible. With respect to the interaction nature

Table 1
Degree of crystallinity, optical energy gap [E_g^{DM} and E_g^T], SPR position, absorbance at SPR position, number of carbon atoms (M), Urbach energy E_u, refractive index (n) and activation energy (E_a) for pure blend PEO/PVP sample and PEO/PVP/Au nanocomposite without and with exposure to gamma irradiation at different doses.

| Samples	Degree of crystallinity (%)	E_g^{DM} (eV)		E_g^T (eV)	SPR position (nm)	Absorbance at SPR position	M	E_u (eV)	n	E_a (kcal/mol)
		E_{gi}	E_{gd}							
Pure blend	25.95	4.86	5.15	4.70	–	–	3.75	0.31	2.04	325.06
Blend/3.6 mg Au NPs	10.14	2.46	3.60	2.96	537.42	1.78	7.40	0.97	2.56	437.64
1 Mrad	17.32	3.65	4.45	4.78	539.33	1.90	4.99	0.88	2.24	392.94
2 Mrad	21.25	3.92	4.57	3.31	531.00	1.53	4.65	0.81	2.18	394.79
3 Mrad	31.40	4.23	4.67	3.72	531.00	1.50	4.31	0.72	2.12	395.90
4 Mrad	28.75	4.08	4.60	3.38	526.27	1.44	4.46	0.91	2.15	395.98
5 Mrad	14.92	3.09	4.02	2.35	529.65	1.94	5.89	0.94	2.37	404.29
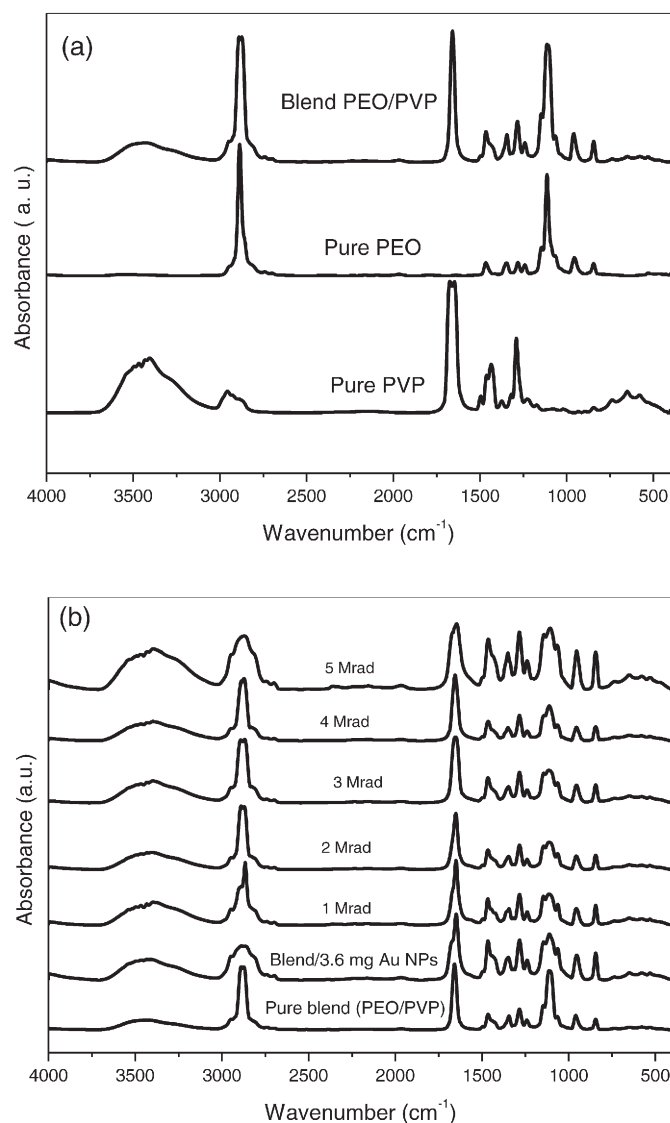
Fig. 3. a–b. FT-IR spectra for pure PVP, pure PEO, pure blend, blend/Au nanocomposite and its irradiation doses (1, 2, 3, 4 and 5 MR).

between PEO/PVP, it is supposed that the quasi hydrogen-bonding exists because of the fact that the hydrogen atoms of PEO possess acidity and the oxygen atoms of carbonyl group of PVP offers electronegativity. A comparison of FT-IR spectra of pristine PEO and PVP with the pure blend spectrum clearly confirms the existence of the hydrogen bonding. The change in the intensity and decrease of broadness of C═O group of PVP exist when it is blended with PEO. This observation explains the effect of forming hydrogen bond between the carbonyl group of PVP and the methylene group of PEO. Also, intensities of the most absorption bands in the spectrum of pure blend sample such as OH, CH_2 and C─O─C stretching vibrations are changed irregularly compared to their values in individual polymers.

From the spectrum of PEO/PVP/Au nanocomposite (0 Mrad) in Fig. 3.b, filling the polymeric matrix of PEO/PVP blend with Au NPs causes largely changes and effects on its functional groups. The intensity and broadness of Hydroxyl group increases after adding Au NPs. The broadness of both CH_2 stretching vibration at 2880 cm^{-1} and C─O─C group at 1110 cm^{-1} increase after filling associated with a decrease in its intensity. This means that there is a strong interaction between ether group of PEO in blend and Au NPs (Fig. 4.a) and results in a distortion in crystalline region in blend which is confirmed by XRD analysis. Also, the intensity of absorption bands at 956 and 845 cm^{-1}

referring to the helical structure of PEO increases after adding Au NPs. The same behavior is also occurred for absorption band in region 1500–1200 cm^{-1}.

The shape of carbonyl group of PVP in PEO/PVP/Au nanocomposite is suffered from a largely deformation associated with a new shoulder at 1665 cm^{-1} which confirms that there is a strong interaction between Au NPs and C═O. The pyrrolidinone adsorbs Au colloid surface preferably via the non-bonding electrons of C═O where the possible interactions of nanoparticles with PVP are listed in our research [27] as shown in Fig. 4.b.

As γ-irradiation dose increases from 1 to 3 Mrad, the intensity of CH_2 stretching band increases accompanied with a decrease in its broadness while the intensity of absorption bands in region 1500–800 cm^{-1} is largely decreased. But the shape of carbonyl group becomes more organized with less deformation. This means that there are structural rearrangements in the chain of PEO/PVP/Au nanocomposite in this region of dose rate which is confirmed by XRD analysis.

With continuous increasing γ-irradiation up to 5 Mrad, the intensity of hydroxyl group and its broadness increases. The intensity of absorption bands in 1500–800 cm^{-1} region is increased largely while the broadness of C═O increases. This is due to cross-linking/chain scission formation by irradiation at high doses that results in an increase in the content of amorphous region in the polymeric matrix. These structural changes and modifications in the polymeric matrix of PEO/PVP after implanting Au NPs and moreover, exposure to γ-irradiation, are in agreement with XRD and UV/vis analyses.

3.3. Ultraviolet and visible analysis UV/vis

Fig. 5.a shows UV/vis absorbance spectra for two basis polymers (PEO and PVP) and pure blend. The spectra show a sharp absorption edge which confirms its semicrystalline nature where it has nearly zero absorption in the wavelength region (300–1000 nm). The spectrum of pure blend shows absorption peak at 215 nm which may be referred to n → π* (R-band) due to containing single bond; so it is thought to absorb radiation only in the far UV region. Fig. 5.b displays UV/vis absorption spectra for pure blend (PEO/PVP), PEO/PVP/Au nanocomposite and its irradiation by γ- rays at different irradiation doses.

From Fig.5b, the spectrum of prepared Au NPs shows absorption peak in the visible region at λ_{max} = 531 nm. The appearance of this peak is due to the surface plasmon resonance (SPR) of Au NPs [2,15, 16] and is the main reason for the striking colors of the different samples. The appearance of this band may be related to the formation of Au NPs by *C. murale* leaf extract. This observation is confirmed by the color change from transparent yellow to a pinkish-red as shown in Fig. 1.

When Au NPs are embedded within the polymeric matrix of PEO/PVP, one can observe that there is a strong increase in the absorbance in the UV/vis regions where the absorption coefficient of filled sample increases and its absorption edge moves toward longer wavelength. The red shift of the absorption edge in the filled PEO/PVP indicates the complexation between the nano-filler and the polymer blend. Also, it reflects the variation in the optical energy gap, which arises because of the change in crystallinity within the polymer matrix [20,26] which was confirmed by XRD analysis. The dramatic enhancement in absorption coincides with the color change of PEO/PVP sample which changes from transparent for pure film to pinkish-red for the nanocomposite sample. The position of SPR peak for nanocomposite film is red shifted to λ_{max} = 537 nm as compared to Au NPs in colloidal solution. This red shift in the position of SPR peak may be due to the increase and/or because of wider size distribution of the NPs within the polymeric matrix. This experimental observation copes with theoretical predictions, which mean that the position of the SPR band of Au NPs embedded in solid polymer matrix shifts to longer wavelengths [28].

As the dose of irradiation process is increased, the intensity of SPR peak is largely decreased and its absorption edge for irradiated sample
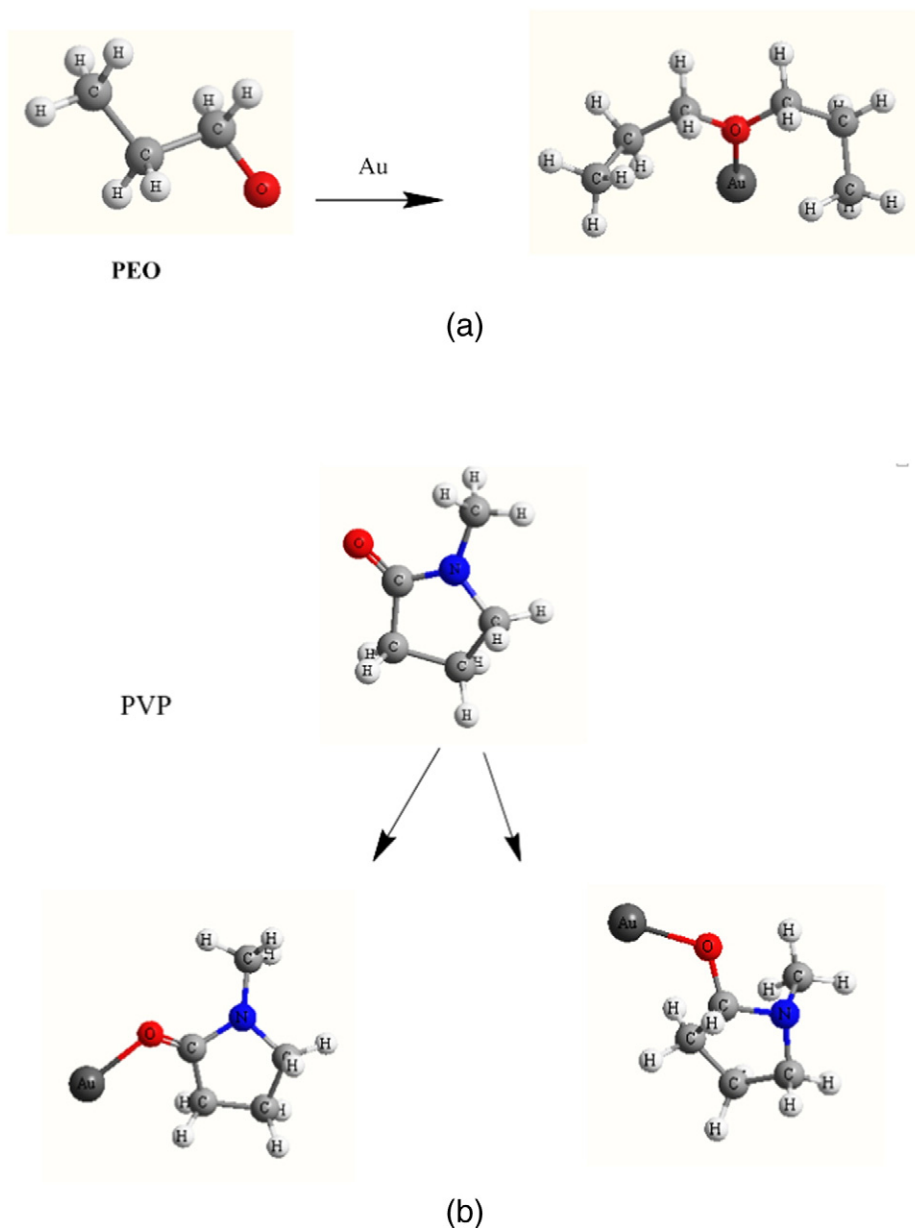
(a)

(b)

Fig. 4. a–b. Suggested modes for interaction Au NPs with PEO and PVP.

is shifted toward shorter wavelengths. This observation indicates that γ-rays cause structural rearrangements in the polymeric matrix where the chains of polymer acquire mobility on the experimental time scale. As the polymer chains relax, stresses are released and an ordered structure is obtained with high degree of crystallinity which is confirmed by XRD analysis. This gives the ability for Au NPs to move again, allowing crystals to agglomerate and/or aggregate which in turn minimizes the absorption band intensity [21]. On the other hand, the increased intensity of SPR peak is related to the increase of the fraction of Au NPs at high irradiation doses 5 Mrad and its location is moved from 536 to 529 nm indicating formation of smaller particles due to its quantum size effect which is also confirmed by TEM micrograph, XRD and FT-IR analysis. This result is due to cross-linking/chain scission within the polymeric matrix of PEO/PVP/Au nanocomposite. The size of particle is likely related to the amount of the stabilizing polymer's chains. With increasing dose of irradiation, the individual macromolecules of PEO/PVP/Au nanocomposite are assumed to be cross-linked with each other. The cross-linking of polymer molecules results in a significant increase in molecular mass. This in turn will increase the

amount of polymer chains surrounding the nanoparticle. The more polymer chains there are, the more they prevent the growth and/or the aggregation of the Au NPs. Also, the increase of irradiation dose will lead to an increase in the rate of nucleation which results in smaller particles formation [21].

3.4. Optical constants

3.4.1. Determination of optical energy gap E_g

The absorption spectrum measurement is the most direct method to investigate and give information about the band structure of materials. In the absorption process, an electron is excited from a lower to higher energy state by absorbing a photon of known energy. The changes in the transmitted radiation can determine the possible electron transitions types.

Davis and Mott [29] reported that near the fundamental band edge, indirect and direct transitions occur and can be observed by plotting $(\alpha h\upsilon)^{1/2}$ and $(\alpha h\upsilon)^2$ versus photon energy $(h\upsilon)$ near the absorption edge for the present experimental data as shown in
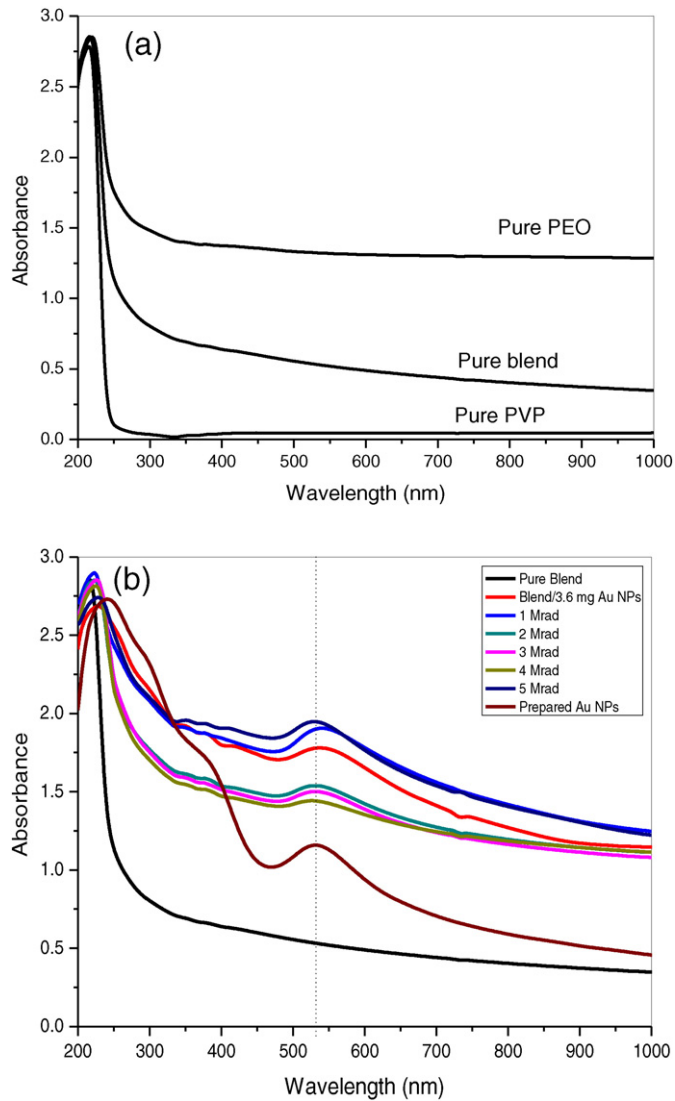
Fig. 5. a-b. UV/vis absorbance spectra for virgin polymers (PEO and PVP), pure PEO/PVP blend, PEO/PVP/Au nanocomposite before and after γ-irradiation process at different irradiation doses.
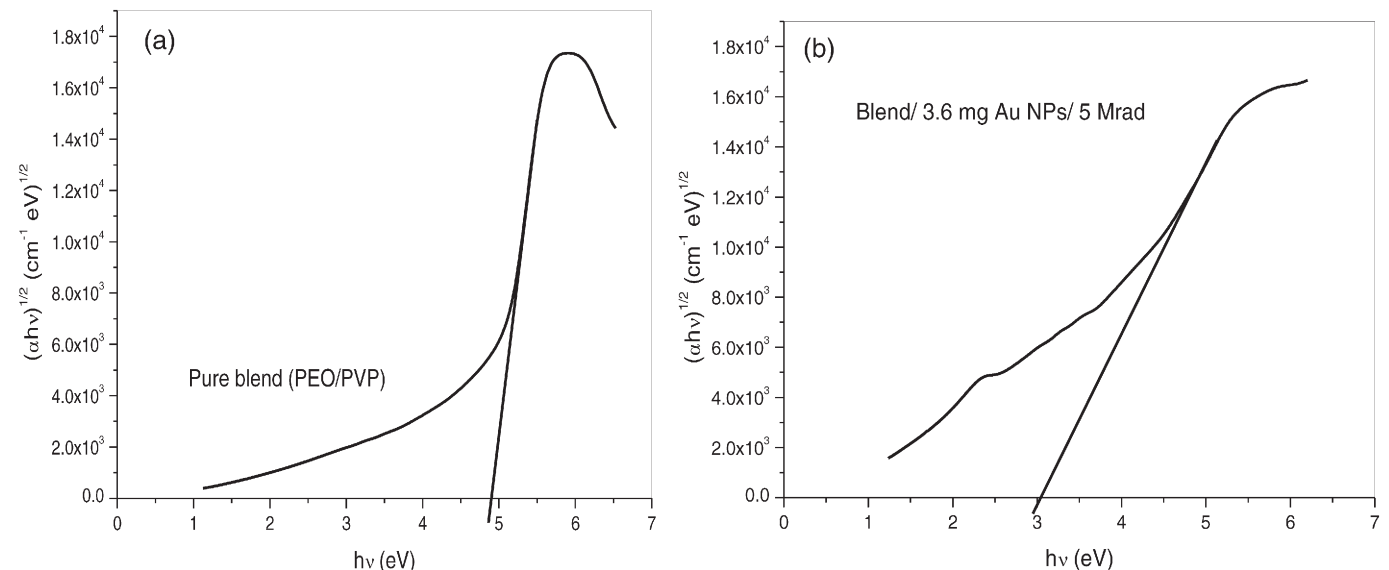
Figs. 6.a–b, 7.a–b for pure blend and one irradiated sample (PEO/PVP/3.6 mg Au NPs/5 Mrad) as an example. Extrapolating the straight parts of these curves to the $h\nu$ axis yields the corresponding forbidden band width (E_g) owing to the following equation:

$$(\alpha h\nu)^{\frac{1}{2}} = B^{\frac{1}{2}} \left(h\nu - E_g\right) \qquad (2)$$

$$(\alpha h\nu)^2 = B^2 \left(h\nu - E_g\right) \qquad (3)$$

where $h\nu$ is the incident photons energy, E_g is the optical energy gap value between the valence band and the conduction band and B is a constant. α is the absorption coefficient and can be calculated from the optical absorption spectrum using the Beer–Lambert's relation [26,30]:

$$\alpha(\nu) = 2.303 \left(\frac{A}{L}\right) \qquad (4)$$

where A is the absorbance and L is the film thickness in cm, is defined by $\log(I_0 / I)$ where I_0 and I are the intensity of the incident and transmitted beams, respectively.

Also, the shift of absorption edge can be related to E_g as follow:

$$E_g = \frac{hc}{\lambda_g} \qquad (5)$$

where h is Plank's constant, c is the speed of light and λ_g is the wavelength that is calculated by using Tauc's expression as follow:

$$\omega^2 A = \left(\hbar\omega - E_g\right)^2 \qquad (6)$$

where $A(\lambda)$ is the absorbance, λ the wavelength of incident light and $\Omega = 2\pi\nu$ is the angular frequency of incident radiation. E_g is deduced from the Tauc's plot of ($A^{1/2} / \lambda$) versus ($1 / \lambda$)) for the same samples, figure not shown. The intersection of the extrapolated spectrum with the abscissa gives the gap wavelength λ_g from which the E_g values are derived. The calculated values of E_g for films by two methods are listed in Table 1.

From this table, it is obvious that the optical energy gap value E_g reduces from 4.86 eV for pure blend to 2.46 eV for blend/Au nanocomposite. This decrease may be attributed to the formation of chemical bonding between the chains of PEO/PVP blend and Au NPs that is the main reason for localized states generation. This indicates that there
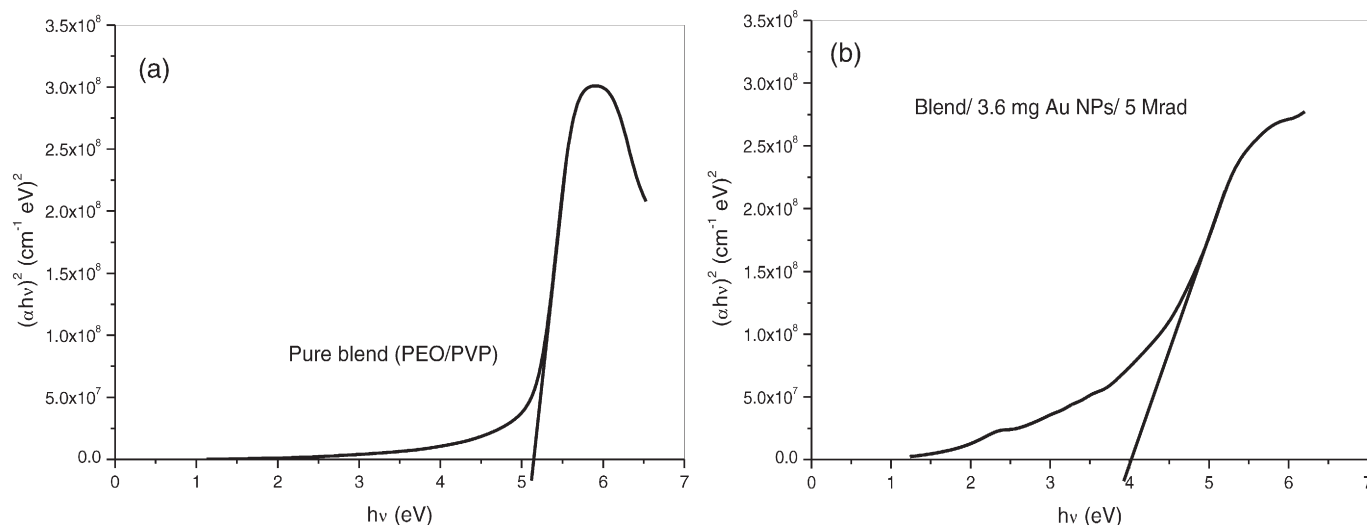

Fig. 6. a–b. $(\alpha h\nu)^{1/2}$ versus photon energy for pure PEO/PVP blend and blend/3.6 mg Au NPs/5 Mrad.

Fig. 7. a–b. $(\alpha h\nu)^2$ versus photon energy for pure PEO/PVP blend and blend/3.6 mg Au NPs/5 Mrad.

are charge transfer complexes CTCs between the highest occupied molecular orbital (HOMO) and the lowest unoccupied molecular orbital (LUMO) energy bands that makes the lower energy transitions feasible. The change in E_g values may be explained by invoking the existence of local cross-linking within the amorphous phase of the polymer blend, in such a way to enhance the disordering degree in these parts as confirmed in XRD analysis [31].

As the dose of γ-irradiation increased (to 3 Mrad), E_g is increased from 2.46 eV to 4.23 eV. This observation is due to improvement for the degree of cystallinity of nanocomposite chains by irradiation process as mentioned in XRD analysis. Polymer ordering results in a significant decrease in molecular mass. This in turn will decrease the polymer chains amount surrounding the NPs. The less polymer chains there are, the more they exhibit the aggregation of Au NPs [21].

With increasing irradiation dose to 5 Mrad, the E_g values are gradually decreased. This result implies that more further irradiation causes the chains to be cross-linked with each other. Thus, this will increase the nucleation rate that leads to smaller particles formation where the intensity SPR peak increases [21]. Further irradiation causes the creation of unsaturated bonds, which are rich in charge carriers (delocalized electrons) and need less energy to endorse electronic transitions between HOMO and LUMO bands [32].

3.4.2. Determination of number of carbon atoms M

The number of carbon atoms (M) in a cluster is related to the optical energy band gap E_g through the modified Tauc's equation:

$$M = \frac{2\beta\pi}{E_g} \qquad (7)$$

where 2β is the band structure energy of a pair of adjacent π sites and β is taken to be -2.9 eV as it is associated with $\pi\rightarrow\pi^*$ optical transition in —C≡C— structure. The obtained M values for pure PEO/PVP, PEO/PVP/Au nanocomposite and its γ-irradiation are listed in Table 1. The value of M for pure blend, which is around 3.75, increases to 7.40 in PEO/PVP/Au nanocomposite. Such an increase can be correlated to the increased conjugation in monomer units of PEO/PVP matrix after the embedding of Au NPs. One notes that the N values increases at high irradiation doses (irradiation dose ˃ 3 Mrad). This is due to breakage of C—H bonds and, in consequence, led to the release of hydrogen. Eventually the surface layer can be transformed into a hydrogenated amorphous carbon with increasing the irradiation dose [33,34]. Thus, carbon enriched domains created in irradiated samples may be responsible for the decreasing in band gap.

3.4.3. Urbach energy E_u

For optical transitions caused by photons of energy $h\nu$ / E_g, the absorption of photons is related to the presence of localized tail states in the forbidden gap. The width of this tail, called the Urbach tail, is an indicator of the defect levels in the forbidden band gap. The following relation was used to calculate the width of the Urbach tail [32,35]:

$$\alpha(\nu) = \alpha_o \exp\left(\frac{h\nu}{E_u}\right) \qquad (8)$$

where α_0 is a constant and E_u is the Urbach energy tail which is interpreted as the width of the tail of localized states in the forbidden band gap. The exponential dependence of $\alpha(\nu)$ on the photon energy h_ν for the samples implies that it obeys the Urbach's formula. For illustrating this dependence, the natural logarithm of the absorption coefficient $\alpha(\nu)$ was plotted as a function of the photon energy h_ν for the studied samples as shown in Fig. 8. The magnitudes of the Urbach energy E_u were estimated and, listed in Table 1, by taking the reciprocal of the slopes of the linear portion in the lower energy region of these curves. From this table, it is obvious that E_u increases from 0.31 for pure blend to 0.97 eV for PEO/PVP/Au nanocomposite. This value gradually decreases with increase in exposure to γ radiations and
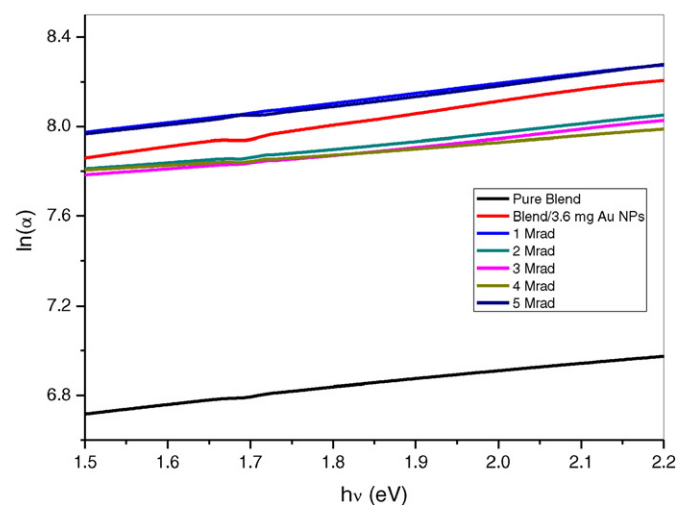

Fig. 8. In (α) versus photon energy plots for pure PEO/PVP blend and its nanocomposite without and with different irradiation doses of γ-rays.

approaches to 0.72 eV for blend/3.6 mg Au NPs/3 Mrad. With continuous increasing the irradiation dose of gamma, the values of E_u increases again up to 0.94 eV for blend/3.6 mg Au NPs/5 Mrad. Such an observation confirms the increase in the traps number as a result of embedded Au NPs and further with exposure to γ-radiation, that results in the lower energy transitions feasible and so that, reducing the optical energy gap values [32].

The variation of the magnitude of E_u in these films, which can be understood by considering the mobility concept as proposed by Davis and Mott [29], indicates that both the filling and irradiation processes significantly affect the Urbach energy E_u where it introduces additional defects within the polymeric matrix. The localized states density was found to be proportional to these defects concentration and consequently Au NPs content and the irradiation dose. The present experimental results concerning the optical energy band gap E_g and the Urbach energy tail E_u imply that filling significantly affects these optical absorption parameters [29].

3.4.4. Refractive index (n)

The change of refractive index 'n' as a function of optical energy gap E_g for pure blend and its nanocomposite without and with different irradiation doses of γ-rays has been studied through the following expression [36]:

$$\frac{n^2-1}{n^2+2} = 1 - \sqrt{\frac{E_g}{20}}. \tag{9}$$

The refractive index dependence n on both Au NPs content and the dose of γ-irradiation is listed in Table 1. It is clear that the refractive index value increases after embedding Au NPs in PEO/PVP matrix and this increase continues with an increase in dose of γ-irradiation. This increase in n of PEO/PVP/Au nanocomposite may be because of the formation of intermolecular hydrogen bonding between Au with the adjacent OH group of PEO/PVP blend which is confirmed by an increase in the intensity of OH in FT-IR analysis [32]. The high value of refractive index is an indication of high density of the film, which leads to a reduction of the inter-atomic spacing. As the dose of γ-irradiation increases to 3 Mrad, the polymeric matrix of PEO/PVP/Au nanocomposite suffers from structural rearrangement leading to decrease in the number of non-bridging oxygen (NBO) bonds. Moreover, high irradiation doses with gamma (from 3 to 5 Mrad) to PEO/PVP/Au nanocomposite films enhances the number of inter-chain interactions, resulting in the change in molecular weight distribution, packing density etc., that results an enhancement in n with irradiation dose. This in turn results in an increase in the average coordination number of the studied composites due to the increase in the number of NBO bonds [37], which increases the refractive index. This increase in refractive index extends the usability of these materials from anti reflection coating for solar cells to high refractive index lenses and has an application in opto-electronics field. The quantitative measurements of these parameters may help in tailoring and modeling of the properties of such nanocomposites for their use in optical devices.

3.5. Transmission electron microscope TEM

The typical TEM micrographs and the corresponding size distribution histograms of biosynthesized Au NPs by *C. murale* leaf extract and blend/Au nanocomposite before and after irradiation process by γ-rays (5 Mrad) are shown in Fig. 9. It can be observed from TEM micrograph of Au NPs in all studied samples that Au NPs are almost spherical in shape. From the histogram of prepared Au NPs, it shows average particle diameters ranged from 2 to 22 nm which is confirmed by the broadness of its SPR peak in UV/vis spectrum. For blend/Au nanocomposite, TEM micrograph confirms the dispersion of Au NPs uniformly in the polymeric matrix but the average diameters of Au NPs are increased to the range 1–34 nm as shown in its histogram. This

observation is confirmed by the red shift of SPR peak in UV/vis analysis that implies that there is wider size distribution of the NPs within the polymer and/or there is an increase in the particle size [28]. The particle size range is decreased to 4–22 nm for blend/Au nanocomposite/5 Mrad sample. This result shows that the particle size distribution is improved for high irradiation doses. However, the observed particles are slightly deviated from spherical symmetry [21]. This may be arisen from the interaction of Au NPs with blend/Au nanocomposite matrix [28]. Finally, the results of TEM behave in good agreement with previously recorded UV/vis analysis.

3.6. Thermogravimetric analysis (TGA)

Thermal stability of a polymer electrolyte is very essential for a safe and endurable electrochemical cell. During the cell reactions, heat is known to get generated in the cell which can melt or degrade the polymer electrolyte within the cell and make internal short circuits. Thus, TGA analysis is very important to investigate the thermal stability of polymeric systems under application conditions. The TGA thermograms of residual weight as a function of temperature for pure, blend/Au nanocomposite and blend/Au nanocomposite/1–5 MR at a heating rate of 10 °C/min in the temperature range from 16 to 700 °C are shown in Fig. 10. The existence of Au NPs in PEO/PVP blend besides exposing to γ-rays does not affect degradation mechanism itself, but has influence on overall thermal stability of the blend matrix.

Pure blend is thermally stable up to 351.82 °C where the solvent is evaporated. On the other hand, the main weight loss is observed in the range of 351.82–455.94 °C. This may be correspondent to the breakdown of polymer backbone and its structural decomposition [26]; and leaving a high amount of residues. The dominant processes appeared during this stage is elimination of OH groups and chain-scission reactions. For degradation step between 455.94 °C and 700 °C, the chain-scission reaction and reactions of intramolecular and intermolecular cyclization and condensation are prevailed until the sample is completely roasted.

When Au NPs are added, the weight loss is decreased and TGA curve moves toward lower temperature ranges. This is due to the high flexibility acquired by the blend after adding Au NPs where the amorphous content increases. Also, this decrease in the degradation temperatures can be attributed to NPs' agglomeration above the optimum loading value [38] as confirmed in TEM micrographs. Fig. 11 summarizes the decomposition temperature versus irradiation dose at different values of the weight loss (10%, 20%, 30%, 40%, 50%, 60% and 70%) for the investigated samples. It can be noticed that the values of temperature increase after exposing samples to γ-rays where the thermal decomposition of irradiated samples moves towards higher temperature ranges than in blend/Au nanocomposite (0 Mrad) implying the enhancement of polymer thermal stability. By comparing the final weight losses values, it can be observed that, the value of blend/Au nanocomposite sample was less than that of the irradiated samples. This enhancement indicates the occurrence of cross-linking in the matrix as a result from the radiation effects and in consequence the polymeric matrix increases in thermal stability.
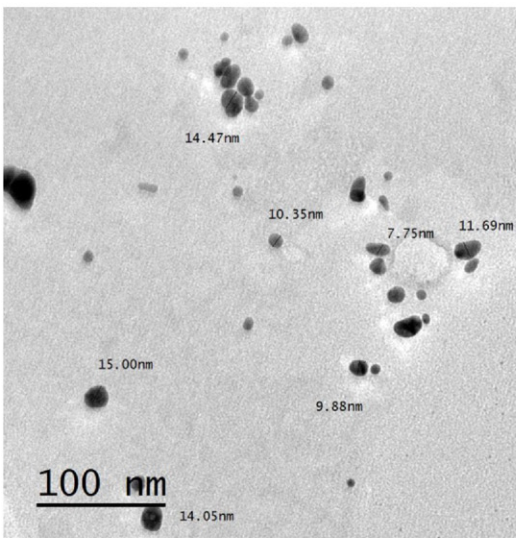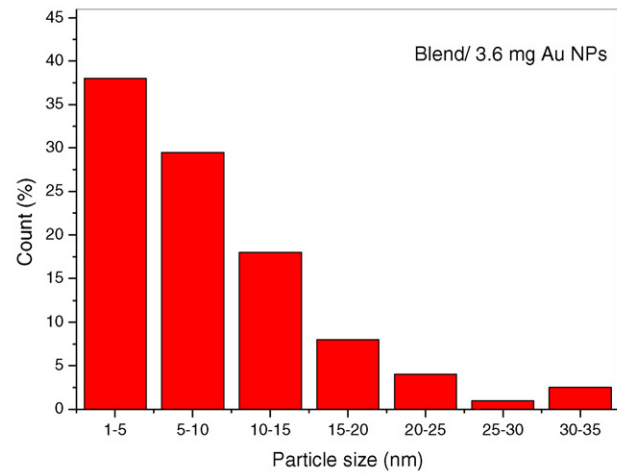
Here, the degradation behavior of blend/Au nanocomposite/1–5 Mrad nanocomposites can be viewed in terms of the ability of free radical diffusion in the polymer matrix that resulted from irradiation process. Chain scission is a result of free radical diffusion among polymer chains; the chains with decreased mobility provide a physical barrier that minimized the diffusion of free radical, so that the polymer decomposition is delayed. The reducing in the chains' mobility can be assigned to the fine dispersion of Au NPs into the polymer matrices and, thus, high surface area of a non-degradable material, which also prevent the macromolecular chains from thermal degradation. Also, delaying in degradation process for irradiated samples, especially blend/Au nanocomposite/4–5 Mrad samples can be assigned to finer dispersion of Au NPs that behaved as efficient
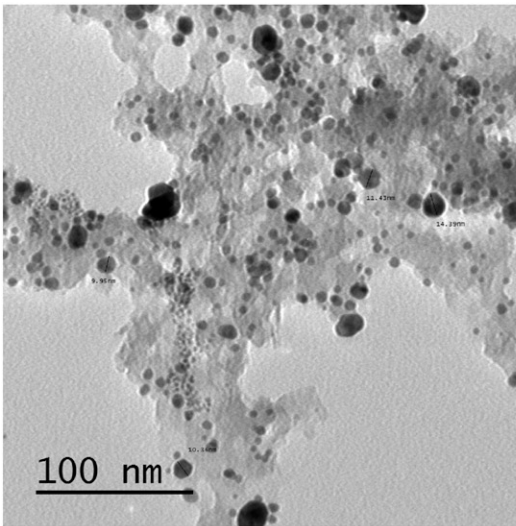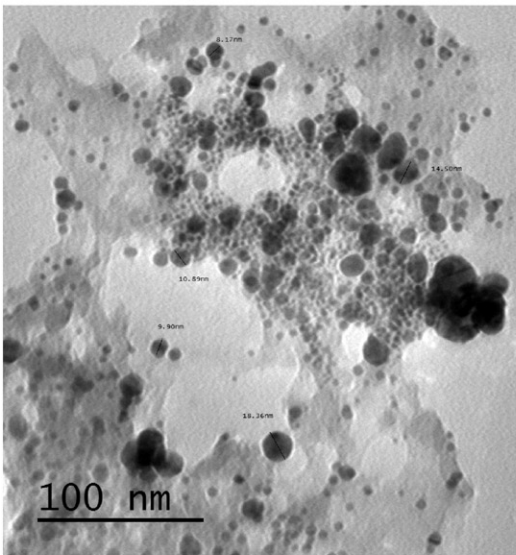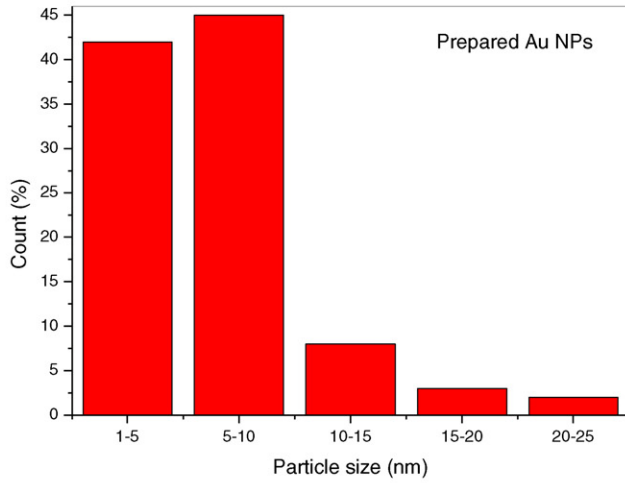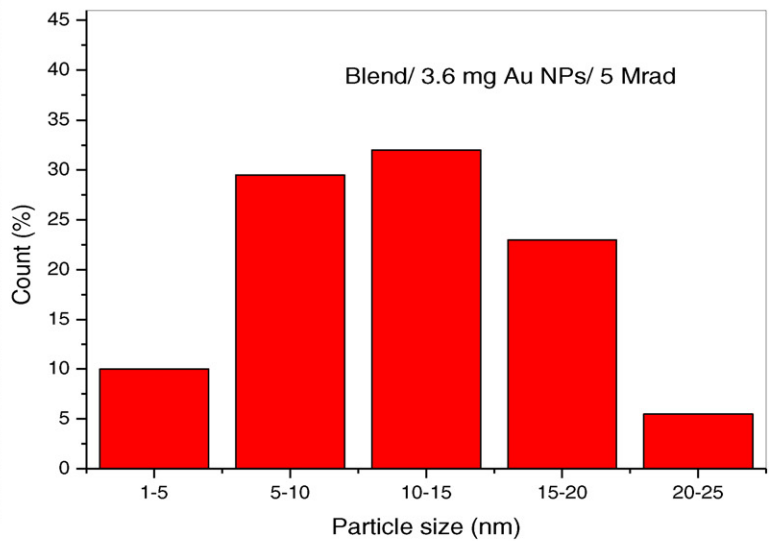
Fig. 9. TEM micrographs for prepared Au NPs, blend/3.6 mg Au NPs and blend/3.6 mg Au NPs/5 Mrad.
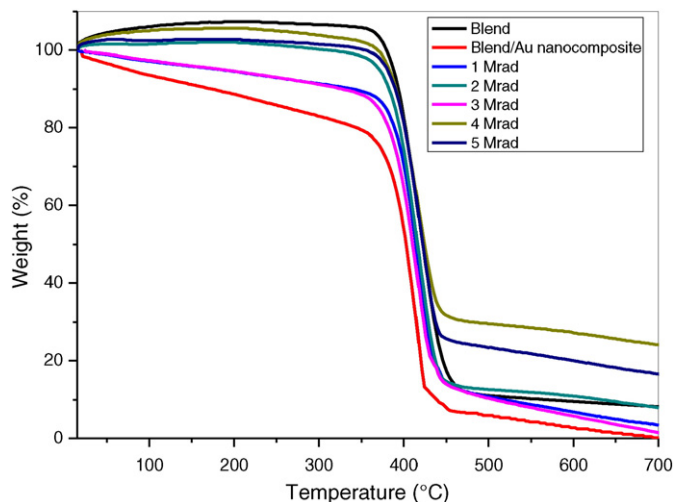
Fig. 10. TGA curves for pure blend and its nanocomposite before and after γ-irradiation at different doses (1, 2, 3, 4 and 5 MR).

heat sinks. Thus, blend/Au nanocomposite/1–5 Mrad will consume more heat than the matrix of blend/Au nanocomposite and does not allow the accumulation of heat within the latter, and thereby prevents oxidation at the early stages of degradation.

3.6.1. Determination of the activation energy E_a

Coats-Redfern model is used to obtain reliable kinetic information on the thermal degradation of pure blend, blend/Au nanocomposite and blend/Au nanocomposite/1–5 Mrad [39]:

$$\log\left[\frac{1-(1-\alpha)^{1-n}}{T^2}\right] = \log\frac{R}{Ea}\left[1-\frac{2RT}{Ea}\right] - \frac{1}{2.303}\frac{Ea}{RT} \quad (10)$$

where n is the order of reaction, T is the absolute temperature, E_a is the activation energy in J/mol, R is the universal gas constant (8.3136 J/mol K) and α is the fractional weight loss at that particular temperature calculated as:

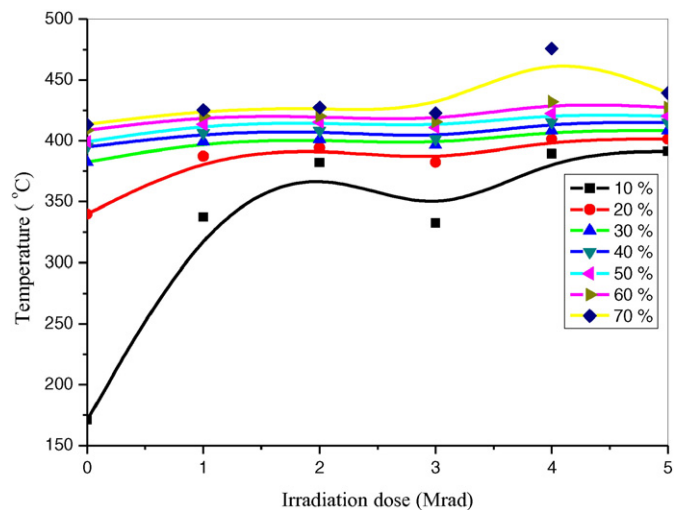$$\alpha = \frac{w_i - w_t}{w_i - w_f} \quad (11)$$

Fig. 11. Decomposition temperatures taken from the TGA curves versus irradiation dose at different values of percentage weight loss (10%, 20%, 30%, 40%, 50%, 60% and 70%) for blend/Au nanocomposite (0 Mrad) and blend/Au nanocomposite/1–5 Mrad.

where w_i is the initial weight, w_t is the weight at given temperature and w_f is the final weight of the sample.

For $n \neq 1$, Eq. (10) reduces to:

$$\log\left[\frac{-\log(1-\alpha)}{T^2}\right] = \log\frac{R}{Ea}\left[1-\frac{2RT}{Ea}\right] - \frac{1}{2.303}\frac{Ea}{RT}. \quad (12)$$

By plotting $-\log[\frac{-\log(1-\alpha)}{T^2}]$ versus $\frac{1000}{T}$ for each sample, we have straight line as shown in Fig. 12. The activation energy values E_a were calculated from the slope of the plot as:

$$E = 2.303R \times slope. \quad (13)$$

The calculated activation energies for the prepared samples are listed in Table 1, where it is obvious that the values of the activation energy are increased from 325.06 to 437.64 kcal/mol for blend/Au nanocomposite. But, E_a values of irradiated samples are less than that of blend/Au nanocomposite where the value of E_a increases with increasing the irradiation dose from 1 to 5 Mrad. These results indicate that both Au NPs and γ-rays are intensively affect the polymer structure.

4. Conclusion

The (PEO/PVP) blend/Au nanocomposite sample was successfully prepared by casting method and exposed to different doses of γ-radiations. The reduction and broadening in the intensity of the main peaks in XRD analysis with the addition of Au NPs to the blend polymer host and exposing to high irradiated doses (4 and 5 Mrad) confirmed the increase in its amorphous nature. XRD analysis revealed the presence of Au NPs in (FCC) crystal structure and the decrease of crystallinity fraction for nanocomposite and high irradiated samples. FT-IR analysis confirmed that the main polar groups of blend, C—O—C of PEO and C=O of PVP, were largely affected due to Au NPs adding and irradiation process. The UV/vis spectra confirmed the formation of Au NPs through the existence of SPR band at 537.42 nm which was shifted to shorter wavelengths 529.65 nm associated with an increase in the absorbance intensity for high irradiated doses. These results clearly implied that Au NPs were embedded in PEO/PVP matrix. The optical parameters were varied depending on the irradiation dose. Such a variation in the optical properties may result in optimize the different optical parameters of (PEO/PVP)/Au nanocomposite after controlled dose of γ-irradiation as per specific requirements in the optical coatings, switches, filters etc. TEM micrographs showed an enhancement for the size of Au NPs and its distribution due to high-irradiation doses. TGA curves for high irradiated samples moved towards higher temperatures. This is preferred in solid polymer electrolytes. The TGA thermograms
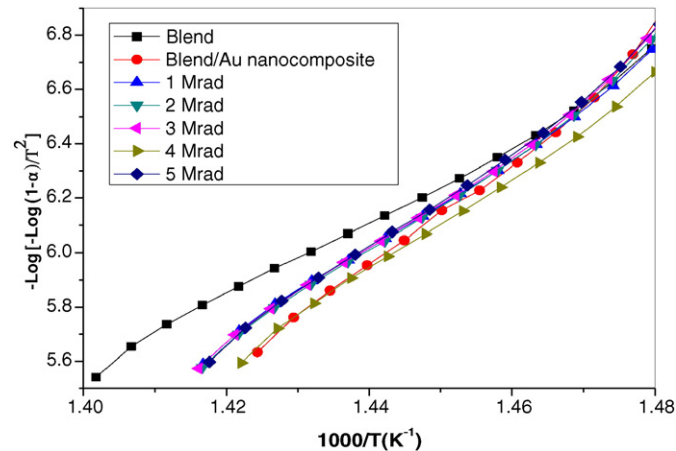

Fig. 12. The dependence of $-\log[\frac{-\log(1-\alpha)}{T^2}]$ versus $\frac{1000}{T}$ for PEO/PVP blend, blend/Au nanocomposite and blend/Au nanocomposite/1–5 Mrad.

for high irradiated samples shifted toward higher temperatures and the values of activation energy were increased for irradiated-nanocomposite samples as compared to nanocomposites.

References

[1] S. Fateixa, A.L. Daniel-da-Silva, N. Jordão, A. Barros-Timmons, T. Trindade, Effect of colloidal silver and gold nanoparticles on the thermal behavior of poly (t-butyl acrylate) composites, Colloids Surf. A Physicochem. Eng. Asp. 436 (2013) 231–236.

[2] M.S. Abdel-Aziz, A. Hezma, Spectroscopic and antibacterial evaluation of nano-hydroxapatite polyvinyl alcohol biocomposite doped with microbial-synthesized nanogold for biomedical applications, Polym.-Plast. Technol. Eng. 52 (2013) 1503–1509.

[3] V.D. Mote, Y. Purushotham, B.N. Dole, Structural, morphological, physical and dielectric properties of Mn doped ZnO nanocrystals synthesized by sol–gel method, Mater. Des. 96 (2016) 99–105.

[4] J. Li, S. Zivanovic, P.M. Davidson, K. Kit, Characterization and comparison of chitosan/PVP and chitosan/PEO blend films, Carbohydr. Polym. 79 (2010) 786–791.

[5] K. Kiran Kumar, M. Ravi, Y. Pavani, S. Bhavani, A.K. Sharma, V.V.R. Narasimha Rao, Electrical conduction mechanism in NaCl complexed PEO/PVP polymer blend electrolytes, J. Non-Cryst. Solids 358 (2012) 3205–3211.

[6] K. Kumar Kumar, M. Ravi, Y. Pavani, S. Bhavani, A.K. Sharma, V.V.R. Narasimha Rao, Investigations on PEO/PVP/NaBr complexed polymer blend electrolytes for electrochemical cell applications, J. Membr. Sci. 454 (2014) 200–211.

[7] K.N. Kumar, K. Sivaiah, S. Buddhudu, Structural, thermal and optical properties of Tb^{3+}, Eu^{3+} and co-doped ($Tb^{3+} + Eu^{3+}$): PEO + PVP polymer films, J. Lumin. 147 (2014) 316–323.

[8] N. Misra, J. Biswal, A. Gupta, J.K. Sainis, S. Sabharwal, Gamma radiation induced synthesis of gold nanoparticles in aqueous polyvinyl pyrrolidone solution and its application for hydrogen peroxide estimation, Radiat. Phys. Chem. 81 (2012) 195–200.

[9] C.-C. Chang, P.-H. Chen, C.-M. Chang, Preparation and characterization of acrylic polymer–nanogold nanocomposites from 3-mercaptopropyltrimethoxysilane encapsulated gold nanoparticles, J. Sol-Gel Sci. Technol. 47 (2008) 268–273.

[10] Y. Li, Y. Pan, C. Yang, Y. Gao, Z. Wang, G. Xue, Synthesis and structural control of gold nanoparticles-coated polystyrene composite particles based on colloid thermodynamics, Colloids Surf. A Physicochem. Eng. Asp. 414 (2012) 504–511.

[11] V.V. Vodnik, N.D. Abazović, Z. Stojanović, M. Marinović-Cincović, M. Mitrić, M.I. Čomor, Optical, structural and thermal characterization of gold nanoparticles–poly (vinylalcohol) composite films, J. Compos. Mater. 46 (2012) 987–995.

[12] H. Yin, H. Tang, D. Wang, Y. Gao, Z. Tang, Facile synthesis of surfactant-free Au cluster/graphene hybrids for high-performance oxygen reduction reaction, ACS Nano 6 (2012) 8288–8297.

[13] E.M. Abdelrazek, G. El Damrawi, I.S. Elashmawi, A. El-Shahawy, The influence of γ-irradiation on some physical properties of chlorophyll/PMMA films, Appl. Surf. Sci. 256 (2010) 2711–2718.

[14] M.F. Eissa, M.A. Kaid, N.A. Kamel, The influence of low-and high-linear energy transfers on some physical properties of poly (methyl-methacrylate) samples, J. Appl. Polym. Sci. 125 (2012) 3682–3687.

[15] K.D. Arunachalam, S.K. Annamalai, S. Hari, One-step green synthesis and characterization of leaf extract-mediated biocompatible silver and gold nanoparticles from Memecylon umbellatum, Int. J. Nanomedicine 8 (2013) 1307–1315.

[16] A.D. Dwivedi, K. Gopal, Biosynthesis of silver and gold nanoparticles using Chenopodium album leaf extract, Colloids Surf. A Physicochem. Eng. Asp. 369 (2010) 27–33.

[17] A. Dey, S. Karan, S. De, Effect of nanofillers on thermal and transport properties of potassium iodide–polyethylene oxide solid polymer electrolyte, Solid State Commun. 149 (2009) 1282–1287.

[18] X.-G. Li, I. Kresse, J. Springer, J. Nissen, Y.-L. Yang, Morphology and gas permselectivity of blend membranes of polyvinylpyridine with ethylcellulose, Polymer 42 (2001) 6859–6869.

[19] K.-P. Lee, A.I. Gopalan, P. Santhosh, S.H. Lee, Y.C. Nho, Gamma radiation induced distribution of gold nanoparticles into carbon nanotube-polyaniline composite, Compos. Sci. Technol. 67 (2007) 811–816.

[20] E.M. Abdelrazek, I.S. Elashmawi, S. Labeeb, Chitosan filler effects on the experimental characterization, spectroscopic investigation and thermal studies of PVA/PVP blend films, Physica B 405 (2010) 2021–2027.

[21] W.H. Eisa, Y.K. Abdel-Moneam, Y. Shaaban, A.A. Abdel-Fattah, A.M.A. Zeid, Gamma-irradiation assisted seeded growth of Ag nanoparticles within PVA matrix, Mater. Chem. Phys. 128 (2011) 109–113.

[22] A. Tawansi, A.H. Oraby, E. Ahmed, E.M. Abdelrazek, M. Abdelaziz, Effect of Na-light radiation on the optical gap and crystal structure of $AgNO_3$-diffused PVDF sensor, J. Appl. Polym. Sci. 70 (1998) 1759–1767.

[23] S. Choudhary, R. Sengwa, Dielectric spectroscopy and viscosity studies of aqueous poly (ethylene oxide) and poly (vinyl pyrrolidone) blend, Indian J. Phys. 85 (2011) 1591–1602.

[24] F.A. El-kader, N. Hakeem, I.S. Elashmawi, A. Ismail, Enhancement of structural and thermal properties of PEO/PVA blend embedded with TiO_2 nanoparticles, Indian J. Phys. 87 (2013) 983–990.

[25] K. Kiran Kumar, M. Ravi, Y. Pavani, S. Bhavani, A.K. Sharma, V.V.R. Narasimha Rao, Investigations on the effect of complexation of NaF salt with polymer blend (PEO/PVP) electrolytes on ionic conductivity and optical energy band gaps, Physica B 406 (2011) 1706–1712.

[26] E.M. Abdelrazek, I.S. Elashmawi, A. El-Khodary, A. Yassin, Structural, optical, thermal and electrical studies on PVA/PVP blends filled with lithium bromide, Curr. Appl. Phys. 10 (2010) 607–613.

[27] A.M. Abdelghany, M.S. Mekhail, E.M. Abdelrazek, M. Aboud, Combined DFT/FTIR structural studies of monodispersed PVP/gold and silver nano particles, J. Alloys Compd. 646 (2015) 326–332.

[28] I. Saini, J. Rozra, N. Chandak, S. Aggarwal, P.K. Sharma, A. Sharma, Tailoring of electrical, optical and structural properties of PVA by addition of Ag nanoparticles, Mater. Chem. Phys. 139 (2013) 802–810.

[29] E. Davis, N. Mott, Conduction in non-crystalline systems V. Conductivity, optical absorption and photoconductivity in amorphous semiconductors, Philos. Mag. 22 (1970) 0903–0922.

[30] A.M. Abdelghany, E.M. Abdelrazek, D. Rashad, Impact of in situ preparation of CdS filled PVP nano-composite, Spectrochim. Acta A Mol. Biomol. Spectrosc. 130 (2014) 302–308.

[31] H. Ragab, Spectroscopic investigations and electrical properties of PVA/PVP blend filled with different concentrations of nickel chloride, Physica B 406 (2011) 3759–3767.

[32] R.P. Chahal, S. Mahendia, A. Tomar, S. Kumar, γ-Irradiated PVA/Ag nanocomposite films: materials for optical applications, J. Alloys Compd. 538 (2012) 212–219.

[33] A. Abdul-Kader, A. Turos, J. Jagielski, L. Nowicki, R. Ratajczak, A. Stonert, M.A. Al-Ma'adeed, Hydrogen release in UHMWPE upon He-ion bombardment, Vacuum 78 (2005) 281–284.

[34] A. Abdul-Kader, Photoluminescence and optical properties of He ion bombarded ultra-high molecular weight polyethylene, Appl. Surf. Sci. 255 (2009) 5016–5020.

[35] F. Urbach, The long-wavelength edge of photographic sensitivity and of the electronic absorption of solids, Phys. Rev. 92 (1953) 1324.

[36] V. Dimitrov, T. Komatsu, Classification of simple oxides: a polarizability approach, J. Solid State Chem. 163 (2002) 100–112.

[37] M. Abdelaziz, Optical and dielectric properties of poly (vinylacetate)/lead oxide composites, J. Mater. Sci. Mater. Electron. 23 (2012) 1378–1386.

[38] S.A. Mansour, Study of thermal stabilization for polystyrene/carbon nanocomposites via TG/DSC techniques, J. Therm. Anal. Calorim. 112 (2013) 579–583.

[39] A. Coats, J. Redfern, Kinetic parameters from thermogravimetric data, Nature 201 (1964) 68–69.